The Role Of Analog-to-Digital Converter Based Mechanical Data Acquisition For Mineral Geological Exploration

Zhongxiao Wei*

Hebi Automobile Engineering Professional College, Hebi 458030, China

*Corresponding author. E-mail: WeiZhongxiao_w@outlook.com

Received: July. 29, 2026; Accepted: July. 08, 2026

Mineral geological exploration requires mechanical data to be collected and analyzed. To process these data effectively, the mechanical data acquisition method based on analog-to-digital converter is adopted in the experiment and optimized. In the experiment, integrated empirical modal decomposition is used for noise reduction processing of data signals, and convolutional neural network is used for feature identification and classification processing of data. After performance validation, for the Analog-to-digital Converter (ADC) based mechanical data acquisition method, the amplitude error between the standard signal and the test signal is between 0.7% and 3.1%, and the frequency error is from 0.05% to 0.30%. After optimization, the proposed method has the lowest final loss value of 0.075. it has the highest accuracy of 99.2%. Also, the proposed method has the lowest Mean Absolute Error (MAE) and Root Mean Squared Error (RMSE) values among all models with 0.38% and 0.094% respectively. In conclusion, the proposed method can effectively process the mechanical acquisition data in mineral geological exploration, which is favorable to the application of ADC-based mechanical data acquisition method in mineral geological exploration

Keywords: ADC; Data acquisition; Geological exploration; Wireless Sensor Networks; Ensemble Empirical Mode Decomposition; Convolutional Neural Networks; Mineral products

http://dx.doi.org/10.6180/jase.202611_34.011

1. Introduction

Mineral geological exploration requires large-scale equipment and data processing support [1]. Among them, mechanical vibration Wireless Sensor Networks (WSNs) are often used for signal acquisition in mineral geological exploration, but the existing WSN has problems such as slow data transmission and insufficient accuracy due to single software and hardware design [2]. As a key component of WSNs, analog-to-digital Converter (ADC) can convert Analog signals into Digital signals with high precision, and can be flexibly configured to adapt to different signal sources and application requirements [3]. However, traditional ADC data acquisition methods have problems such as noise interference, difficulty in synchronous acquisition of multi-source signals and low data processing efficiency when processing complex mechanical signals [4]. To solve these problems, a mechanical data acquisition method based on ADC is proposed. It is optimized by combining Empirical Mode Decomposition (EEMD) and Convolutional Neural Networks (CNN). ADC is used to collect mechanical vibration signals in mineral geological exploration and convert them into digital signals. Then, EEMD is used to preprocess the collected signals, remove noise and extract key features. Finally, the feature extraction and classification of the processed signals are carried out in combination with CNN. This study aims to address the synchronization, noise suppression, and classification accuracy issues of multi-source vibration signal acquisition in complex exploration environments through collaborative optimization of system architecture and algorithms, thereby promoting the development and application of technology in this field. The innovation of this study lies in: (1) A synchronous acquisition architecture based on path aware time compensation and double buffering mechanism is proposed, which solves the asynchronous triggering problem of multi node acquisition commands caused by transmission path differences at the protocol level. (2) The study develops a signal collaborative processing framework that integrates EEMD adaptive noise injection and Intrinsic Mode Function (IMF) correlation coefficient screening, achieving seamless integration from signal denoising to CNN feature classification. The main contributions of this study are as follows: (1) A complete mechanical vibration signal processing chain was established, covering multi-node synchronous acquisition, adaptive noise suppression, and feature classification. (2) A dual-buffer combined with DMA data storage mechanism was designed, which alternately switches between buffers and directly stores the data into the SD card, avoiding data overflow and interruption during acquisition. Unlike existing research, which primarily focuses on enhancing ADC hardware metrics or optimizing a single algorithm, this paper introduces a distinct approach. This method systematically addresses the three major engineering challenges that limit data acquisition accuracy and efficiency: multi-source asynchronous acquisition, strong noise interference, and inefficient signal classification. It achieves this through collaborative design at both the system and algorithm levels, without modifying the core conversion hardware, and by implementing an innovative peripheral system synchronization architecture alongside backend collaborative processing algorithms.

2. Related works

WSNs can be used for mechanical data acquisition and transmission in mineral geological exploration processes [5]. Chaudhari applied different optimization methods to the data processing of WSNs so as to verify the ability of different methods to solve the security problems. These results confirmed that swarm intelligence algorithms could effectively improve the security of data transmission in WSNs [6]. To prevent duplicate categorization of data, Suganya and Sountharrajan proposed an integrated approach based on clustering algorithm. The results confirmed that this method maintained the efficiency of the network and improved the energy utilization [7]. Elsway et al. confirmed that the processing of data in WSNs can be optimized using the whale optimization algorithm, which leads to energy regulation and improves the lifetime of WSNs. The results confirmed that this optimization method outperformed the baseline model and showed high stability [8].

ADC is an important component of WSNs hardware module for signal processing. Chakravarthi and Chandramohan introduced concepts such as sampling time in ADC. They combined several parallel ADC for receiving and processing signals in the same time period. In these simulation experiments, this parallel ADC was able to significantly improve the accuracy of data processing [9]. Huang et al. used a deep neural network to continuously train the parameters involved in the ADC to obtain a combined software and algorithmic optimization method. The results confirmed that the method was able to utilize the algorithm to improve the storage and data processing capabilities of the ADC [10]. Yanbo et al. combined a noise processing function with a feed forward network for reducing the effect of noise in the ADC. The simulation results confirmed that this combined approach improved the efficiency of noise processing and was able to solve the low resolution problem in ADC [11]. Sardar et al. introduced an adaptive approach to ADC for data retrieval. The simulation results confirmed that the optimization method enabled efficient transformation of resources, thus increasing their utilization [12]. Bashir et al. proposed a new ADC hybrid architecture for optimizing parametric design. In these simulation experiments, the architecture was able to increase the resolution of the circuit, resulting in more accurate data output [13].

To sum up, the existing data collection and processing methods have obvious deficiencies in mineral geological exploration. For example, the mechanical vibration signal acquisition based on WSNs is slow and inaccurate due to the single hardware and software design. Although some optimization methods can improve the efficiency of data processing, they can not effectively solve the problem of noise interference of complex mechanical signals and synchronous acquisition of multi-source signals. In addition, most of the existing ADC optimization researches are limited to hardware design or single algorithm optimization, which fails to combine complex signal processing and deep learning techniques to meet the high precision requirements. Therefore, this paper combines EEMD and CNN, and uses EEMD for noise reduction and signal classification. Secondly, the dual buffer mechanism and synchronous trigger method are used to optimize the synchronous acquisition of multi-source signals to solve the problem of asynchronous signal acquisition and data loss in the traditional method.

3. Methods

This article proposes a mechanical data acquisition method based on ADC, and optimizes it by combining EEMD and CNN. The core of this study is to construct a complete signal processing pipeline and system control strategy tailored to the characteristics of exploration vibration signals. In the aspect of system control, the research method mainly focuses on how to optimize the hardware and algorithm of ADC to ensure the synchronous acquisition. In response to the shortcomings of ordinary ADC in synchronous acquisition and anti-interference, this study optimizes their clock synchronization mechanism and peripheral circuit design from a hardware perspective, and introduces double buffering and path aware time compensation strategies from an algorithm perspective to ensure high-precision synchronous acquisition of multi-source data in complex exploration environments. A system based on WSN is designed, which includes acquisition, routing and gateway nodes, and uses multi-mode multiplexing technology to process mechanical vibration data. The sensor uses a sampling rate of 10KHz to meet the Nyquist theorem's requirements for collecting typical vibration signals ($\leq$ 5KHz). The Central Processing Unit (CPU) generates Pulse Width Modulation (PWM) frequency for ADC configuration, and the timer frequency is set to 160 MHz, which is an integer division of the system's main frequency to provide high-precision timing reference for mechanical vibration data processing. An advanced timer implementation based on STM32F4 series microcontroller (MCU), with a clock division accuracy of up to 8.4 ns, provides a low jitter and high stability timing reference for PWM driven ADC sampling clock. To solve the data transmission delay, the path sensing time measurement and compensation technology is introduced, and the continuity of data acquisition is ensured by double buffering mechanism. The ensemble EEMD was used for data noise reduction, and the CNN was combined for feature extraction and classification.

The performance of the model was optimized by batch normalization and loss function.

3.1. ADC-based mechanical data acquisition methods

ADC needs to have high resolution to accurately capture weak signal details, high sampling rate to fully record complex frequency components of the signal, and high throughput capability to process massive data streams [14]. In response to the shortcomings of existing WSNs in mineral geological exploration sites in dealing with such multi-source and strong noise data, this study designs a multi-mode multiplex WSNs hardware transmission system. In the whole transmission system, it mainly includes acquisition, routing and gateway nodes. The acquisition node is dominated by the CPU, and circuits such as sensors, power management, and signal differentials are distributed around it. The routing node is mainly composed of two mode 1 processors. The gateway node contains one mode processor. The gateway node contains one mode processor. Fig. 1 shows the specific structure of this transmission system.

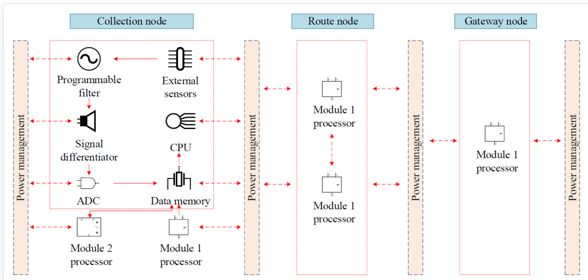

Fig. 1. Hardware transmission system for WSNs with multimode multiplexing

In Fig. 1, the CPU is the core of the acquisition node, which is used to initialize the file system, program status lights, selection of acquisition signals, high-quantization ADC data acquisition, sampling time, and sampling rate. The CPU coordinates the working timing of various peripheral devices by configuring internal registers and control logic. Specifically, the CPU generates corresponding PWM signals to drive the ADC based on the set sampling rate, controls the sampling interval through a timer, and uses Direct Memory Access (DMA) mechanism to achieve dual buffering parallel processing of data acquisition and storage operations, thereby ensuring the continuity and real-time performance of data acquisition. The sampling rate of the acquisition node, controlled by the CPU, is set to 10 KHz in experiments. This setting meets the requirements of the Nyquist sampling theorem, ensuring that typical mechanical vibration signals up to 5KHz in mineral geological exploration sites can be collected without distortion. The sampling rate is configured alongside parameters like 1024-point sampling length, 20 mV voltage, and 1.15×10^6kbps computer-network management node communication rate. This rate matches the demand for capturing complex mechanical vibration signals in mineral geological exploration, ensuring sufficient data density for subsequent EEMD denoising and CNN-based feature analysis. External sensors can realize the conversion of mechanical signals to electrical signals. Data converter can realize the conversion of analog signal and digital signal. The data memory can store the converted digital signals in the Secure Digital (SD) card under the control of the CPU [15]. In this system, software control of programmable filters is its core. The CPU sends control commands to the configuration register of the filter chip through digital communication interfaces such as SPI/I2C, dynamically setting parameters such as cutoff frequency, filter type, and roll off slope. The control software automatically calculates and updates the filtering parameters based on the preset mechanical vibration signal frequency band model or real-time spectrum analysis results, thereby achieving adaptive filtering and noise suppression for different mineral vibration characteristics. Programmable filters set their bandwidth to 1 Hz to 5 kHz based on the frequency characteristics of mechanical vibration signals, effectively filtering out excess noise signals outside of this frequency band. Two types of mode processors are used for data transmission. The mode 1 processor (based on the IEEE802.11 standard protocol) is the main structure, which commands and feeds the data and transmits the real signals. The mode 2 processor (based on IEEE802.15.4 standard protocol) is the secondary circuitry used to assist in network formation in complex environments. Eq. (1) is the PWM frequency generated by the CPU when configuring the ADC f_{MCLK}.

$$f_{\mathrm{MCLK}} = 16 f_{\mathrm{samp}} \tag{1}$$

In Eq. (1), f_{samp} denotes the sampling frequency of the ADC. Eq. (2) extends the operation of f_{MCLK}.

$$f_{MCLK} = \frac{2^{\mathrm{ClockDivision}} \cdot f_{\mathrm{TimerClock}}}{(1 + T_{\mathrm{Period}})(1 + T_{\mathrm{Prescaler}})} \tag{2}$$

In Eq. (2), ClockDivision denotes the crossover coefficient of the timer set in the CPU, which is set to 0. $T_{\mathrm{Prescaler}}$ denotes the prescaler coefficient, which is set to 0. $f_{\mathrm{TimerClock}}$ denotes the frequency of the timer, which is set to 160MHz.T_{Period} denotes the clock period. Eq. (3) can be obtained by substituting the above parameters into Eq. (3).

$$T_{\mathrm{Period}} = \frac{160 \times 10^6}{f_{\mathrm{MCLK}}} - 1 \tag{3}$$

Substituting Eq. (1) into the above Equation yields Eq. (4).

$$T_{\mathrm{Period}} = \frac{10 \times 10^6}{f_{\mathrm{samp}}} - 1 \tag{4}$$

An arbitrary value of T_{Period} was pre-set in the experiment and it was updated only when the data acquisition was formally performed. The data acquisition of WSNs consists of 2 processes, firstly acquiring the data using the ADC and then saving the data. These two steps need to be performed simultaneously to achieve continuity in data acquisition. When encountering complex environments such as ultra-high voltage, data acquisition and transmission are prone to data misalignment and packet loss [16]. When analyzing mechanical acquisition signals, signals from multiple sources need to be processed simultaneously. However, the acquisition commands issued cannot reach the acquisition nodes at the same point in time due to the different paths. To address these issues, a double buffer mechanism and a reliable data transfer protocol are designed in this research for ADC data storage and to guarantee the reliability of data transfer. Firstly, buffers 1 and 2 are defined in the CPU, and they take up a certain amount of operating memory. One buffer is able to store 1024 points of data. Buffers 1 and 2 need to be emptied when starting data acquisition, while the defined timer is set to 1, and then data acquisition is performed. After 1 data point is collected the CPU is notified to place the serial data into buffer 1, at this time the timer is added to 1 . The counter is then judged in relation to 1024, when it is equal to 1 it means that buffer 1 is full, otherwise buffer 1 is not full. If buffer 1 is full, the data should be placed in buffer 2. At this point, the DMA controller acts on buffer 1 to store the data to the SD card. At this point the CPU is able to work on both threads and collect data at the same time. The above steps are repeated and buffers 1 and 2 are switched until acquisition is complete. This effectively solves the data overflow and blocking problem.

Based on this, a synchronized triggering method is proposed in the experiments for acquisition commands to trigger acquisition simultaneously. The core aspect of this method is to obtain the appropriate number of synchronization tests for solving the transmission delay caused by the path. Synchronization processing adopts path-aware time measurement: each line is measured four times-host computer sends test commands, acquisition points time after receiving, cycles until stopping timing, then calculates total time difference for compensation.

Tests with 3 acquisition +1 gateway nodes (10K sampling rate, 1.5×10^5bps baud rate, 100 triggers/node) show 500 tests minimize nodes' compensation/average path time, so 500 is set as test count to solve path-induced transmission delay. There are differences in the transmission path length and hardware delay from different nodes to the host in WSNs, which can cause the collection commands to not arrive synchronously. Path aware time measurement actively calculates and compensates for this inherent delay, theoretically ensuring the synchronous triggering of multi-source acquisition commands in time. Therefore, the path-aware time measurement method is selected in the experiment to compensate the time difference caused by the transmission path. When performing path-aware time measurement, each line is measured four times. The first measurement test command is first issued by the host computer and timed after receiving the command from the acquisition point. The second measurement command is issued when the first timing command is executed. The above steps are repeated until the collection point receives the third instruction to stop timing, and the time difference in the whole process is calculated. Finally, the obtained time difference is input to the terminal device for data processing. During this process, the terminal device utilizes these path delay data to calculate accurate compensation values and integrates them into the synchronization triggering mechanism. In this way, the system can actively eliminate timing errors introduced by inconsistent transmission paths at the protocol level, thereby fundamentally ensuring time consistency in subsequent data acquisition stages. In hardware transmission systems, the CPU is responsible for initializing the file system and controlling the ADC parameters. Sensors convert mechanical vibration signals into electrical signals, and data converters perform analog-to-digital conversion. Programmable filters with cutoff frequencies as required. Sensors typically use piezoelectric or strain sensing units to convert mechanical quantities such as acceleration and displacement caused by mechanical vibrations into continuous analog voltage signals proportional to them. ADC periodically samples and quantizes the analog signal, converting it into a discrete digital sequence that can be processed by a digital system for subsequent digital signal processing and storage. Dual processor redundancy design ensures transmission reliability, and the main communication protocol is IEEE 802.11.

3.2. Optimization of ADC-based mechanical data acquisition methods

In the mechanical data collection for mineral geological exploration mentioned above, the signal is easily contaminated by complex noise such as heavy equipment operation and random electromagnetic pulses on site, resulting in a decrease in accuracy. Therefore, noise reduction of these data is also required. The EEMD method is selected to improve the mode mixing problem of traditional methods due to its adaptive decomposition characteristics, which can effectively handle non-stationary and nonlinear mineral geological exploration vibration signals. The specific completion process is as follows: Firstly, Gaussian white noise with different realizations is added multiple times to the original signal to uniformly fill the entire time-frequency space. Subsequently, each signal with added noise is subjected to EEMD to obtain a set of IMF components. Finally, the corresponding IMF components are averaged overall to offset the impact of added noise and obtain the final IMF. After averaging the signal, Gaussian white noise is added to cancel out the original noise, thus achieving noise reduction. First assume that the original signal to be decomposed is $x(t)$ and its average initialization number is m. Then Gaussian white noise $u_n(t)$ is added to obtain the new time series $Y_n(t)$ in Eq. (5).

$$Y_n(t) = x(t) + u_n(t) \quad n = 1, 2, \ldots, m \tag{5}$$

In Eq. (5), $Y_n(t)$ represents the new time series obtained after adding Gaussian white noise for the nth time. n represents the sequence number for adding noise. Eq. (6) is obtained by discretizing.

$$Y_n(t) = \sum_{i=1}^{K} c_i^n(t) + r_n(t) \tag{6}$$

In Eq. (6), K is the amount of IMF weight. $c_i^n(t)$ represents the i th IMF component from the nth decomposition. $r_n(t)$ represents the amount left after the nth decomposition. The above steps are repeated several times, and the final IMF component in Eq. (7) can be obtained by averaging the IMF components.

$$c_i(t) = \frac{1}{m} \sum_{n=1}^{m} c_i^{(n)}(t) \tag{7}$$

In Eq. (7), $c_i^{(m)}$ is the i _th IMF component obtained by the m_th decomposition. m is the number of decomposition. Fig. 2 illustrates the specific EEMD decomposition steps.

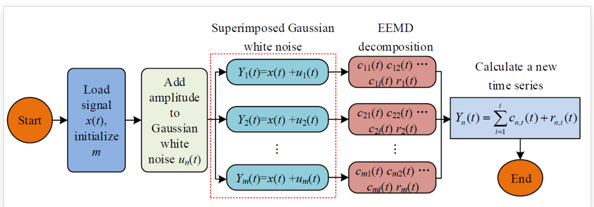

Fig. 2. Specific decomposition steps of EEMD

When applying EEMD to the noise in the mechanical data acquisition for mineral geological exploration, it is necessary to add appropriate Gaussian white noise, otherwise it will increase the computational effort or fail to resolve the modal aliasing. The intensity of the noise needs to be large enough to make the characteristics of the signal more obvious, but not so large that it obsaches the information of the original signal. The amplitude standard deviation calculation of the original signal is expressed in Eq. (8).

$$\varepsilon = \sqrt{\frac{1}{N}\sum_{i=1}^{N}(x_i - \bar{x})^2} \tag{8}$$

In Eq. (8), ε represents the standard deviation of the amplitude of the original signal x_i. x_i is the i th sample value of the signal, $\bar{x}$ is the mean value of the signal, and N is the total number of samples of the signal. According to the noise theory in signal processing, when the noise intensity is one quarter of the standard deviation of the signal amplitude, the

SNR of the signal can be maintained at a high level, and the interference effect of noise can effectively reduce mode aliasing, so $\partial = \frac{\varepsilon}{4}$ is selected [17]. Eq. (9) provides a criterion for adding energy to Gaussian white noise.

$$\begin{cases} \partial = \frac{\sigma_n}{\sigma_o} \\ \varepsilon = \frac{\sigma_h}{\sigma_o} \end{cases} \quad 0 < \partial < \frac{\varepsilon}{2} \tag{9}$$

In Eq. (9), σ_o and σ_n denote the standard deviation of amplitude before and after adding noise, respectively. σ_h denotes the amplitude standard deviation of the high frequency signal components. ∂ and ε is the standard deviation criterion. The cliff method is utilized in the experiment to solve the IMF components, and Eq. (10) shows its calculation method.

$$K = \frac{1}{n}\sum_{i=1}^{n}\left(\frac{x_i - \mu}{\sigma}\right)^4 \tag{10}$$

In Eq. (10), n denotes the length of the collected sample. μ and σ denote the mean and standard deviation of the signal, respectively. The correlation coefficient method is generally used to measure the correlation between IMF components. Eq. (11) shows the calculation of the correlation coefficient R.

$$R = \frac{\mathrm{cov}(x, y)}{\sigma_x \sigma_y} \tag{11}$$

In Eq. (11), x and y are signals. $\mathrm{cov}(x, y)$ denotes the covariance between x and y. σ_x denotes the standard deviation of $x \cdot \sigma_y$ denotes the standard deviation of $y \cdot R$ Components less than 0.3 are generally considered useless and need to be eliminated.

After the collection of data as described above, relevant information about the geology and minerals of the study area can be obtained. It is also necessary to carry out the classification process of them for the classification of minerals, so as to determine the results of geological exploration. The geological data acquisition process: WSNs with multi-mode multiplexing (acquisition/routing/gateway nodes) collect mechanical vibration signals; CPU-controls high-quantization ADC converts signals to digital, stored via dual-buffer; EEMD adds Gaussian white noise, decomposes to IMF, removes components with correlation coefficient <0.3 for denoising [18]; Finally, VGG16 extracts features and classifies to get geological and mineral info. Due to its powerful automatic feature extraction and hierarchical learning capabilities, CNN's convolutional layers effectively capture spatial local patterns and frequency features in signal data, enabling robust classification of mineral type signal variability under common noise and signal variability conditions in mineral geological exploration sites [19]. As a kind of CNN architecture, the VisualGeometry Group 16-layer network (VGG16), whose 16-layer depth structure extracts higher-order features layer by layer through convolution layer and pooling layer, can provide rich detailed information and adapt to complex mineral data [20]. In contrast, although ResNet solves the gradient disappearance problem, it is more complex and easy to overfit. MobileNet is lightweight and efficient but lacks accuracy [21]. Therefore, VGG16 is more advantageous in mineral classification, meeting the needs of high precision and high reliability. Therefore, this model is chosen as the method for mineral classification in the experiment. To ensure the accuracy of classification, the loss function needs to be utilized to reduce the error. The cross-entropy loss function in Eq. (12) was chosen for the experiment.

$$L(W, b) = -\frac{1}{n}[\eta \cdot \log \hat{y} + (1 - y)\log(1 - \hat{y})] \tag{12}$$

In Eq. (12), η is the label value. $_n$ is the sample length. $\hat{y}$ is the output value. W is the weight. b is the bias. The training of the model took forward and back propagation. To prevent overfitting, the batch normalization method is chosen for the experiment. Assuming that the output of l layer neurons is B, the batch normalization method in Eq. (13) can be obtained.

$$\hat{x_m^l} = \frac{x_m^l - \mu_B}{\sqrt{\sigma_\beta^2 + \varepsilon}} \tag{13}$$

In Eq. (13), x_m^l denotes the input value. β is the adjustment parameter of the panning. The output of the batch normalization method is represented by Eq. (14).

$$y_i^l = \gamma x_i^l + \beta \tag{14}$$

In Eq. (14), γ represents the trainable scaling parameter. x_i^l represents the value after batch normalization, which is the middle value after mean zeroing and variance normalization. β stands for trainable translation parameter. To improve the model's ability to fit complex functions, β and the scaling adjustment parameter γ in Eq. (15) are added to the experiments.

$$\widehat{x_m^l} = \frac{x_m^l - \mu_B}{\sqrt{\sigma_\beta^2 + \varepsilon}} \square \gamma + \beta \tag{15}$$

Embedding the batch normalization layer into the activation function yields a special network layer in Eq. (16).

$$a^l = f\left(BN_{\gamma,\beta}\left(x_m^l\right)\right) \tag{16}$$

In the exploration of mineral geology, the study incorporates the data processing methods mentioned above, including data acquisition, noise reduction, and classification. Based on these methods, the ADC-based mechanical data acquisition optimization method in Fig. 3 is established in the experiment.

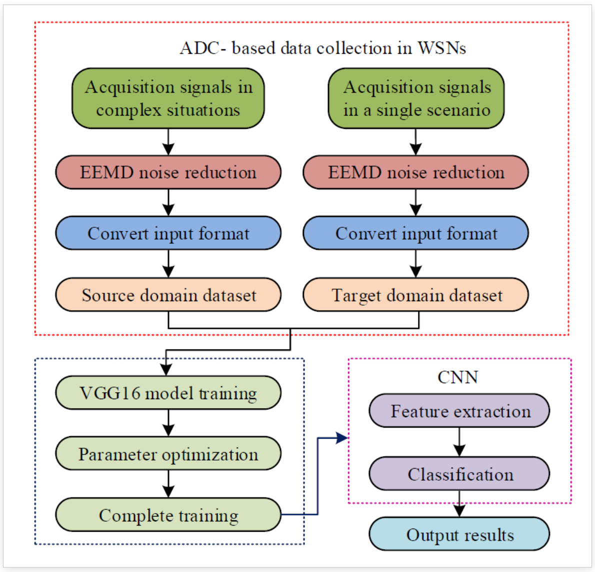

Fig. 3. Optimization method for mechanical data collection based on ADC

In Fig. 3, the data acquisition method adopted in the experiment is WSNs, in which the hardware structure ADC is mainly optimized. The ADC was utilized in the experiment for data acquisition for mineral geological exploration. To improve the accuracy of data acquisition, the study utilized EEMD to process the noise and improve the strength of the signal [22]. Relevant mineral and geological information can be obtained by the above method, and it is necessary to further classify and process these data. Finally, according to the results of model training to determine the type of minerals. Before EEMD decomposition, the original signal needs to be pre-processed, including de-noising and normalization to [-1, 1], in order to reduce the impact of noise interference and amplitude difference on the decomposition. EEMD decomposes the signal into a number of IMF and residual terms, and each IMF satisfies the conditions that the difference between the extreme point and the number of zeros is at most 1 , and the local upper and lower envelope mean is zero. After decomposition, the IMFs with high correlation coefficient are retained to retain important information by calculating the correlation coefficient between each IMF and the original signal. It calculates the correlation coefficient of each IMF with the original signal. The higher the correlation coefficient, the more likely the IMF is to contain useful information about the original signal. The calculation process is shown in Eq. (17).

$$P_{I_i} = \frac{\sum_{t=1}^{N}(x(t)-\bar{x})\left(I_i(t)-\bar{I}_i\right)}{\sqrt{\sum_{t=1}^{N}(x(t)-\bar{x})^2} \cdot \sqrt{\sum_{t=1}^{N}\left(I_i(t)-\bar{I}_i\right)^2}} \tag{17}$$

In Eq. (17), $x(t)$ is the original signal, $I(t)$ is the i th IMF, and $\bar{x}$ and $\bar{I}_i$ are their means respectively. IMFs with a correlation coefficient greater than a certain threshold (such as 0.3 or 0.5) are usually selected as meaningful IMFs. Spectral analysis (such as fast Fourier transform FFT) is performed on each IMF to observe its frequency distribution. Meaningful IMFs usually correspond to a specific frequency component or band in the signal. In summary, this research method can be summarized into three collaborative stages. Firstly, high-precision synchronous acquisition of multi node vibration signals is achieved through path aware time compensation and double buffering mechanism. Secondly, signal denoising is achieved by utilizing EEMD adaptive noise injection and IMF correlation coefficient screening. Finally, the VGG16 network is used to extract features and classify minerals from the denoised time-frequency map.

4. Results and discussion

4.1. Accuracy verification of mechanical data acquisition method based on ADC

To verify the data collection and processing performance of the proposed method in mineral geological exploration related scenarios, the experiment used a publicly available dataset containing multiple mechanical vibration modes for analysis to simulate various vibration sources in the exploration site, including the Kaggle machinery vibration and failure data set (https://www.kaggle.com/datasets/brjapon/mechanical-failure-vibration-d MATLAB ataset), vibration signal sample data sets (https://www.mathworks.com/help/signal/ug/vibration-analysis.html). The following parameters were set in the experiments: sampling length of 1024 points, voltage of 20 mV, communication rate between the computer and the network management node of 1.15 $\times$ 10^6 kbps, sampling rate of 10 KHz, sampling mode of 0x01, node number of 0x00, and checksum code of 0xFF. The periodic impact and harmonic characteristics of the mechanical vibration signals of bearings/gears used in this study can be essentially compared to the elastic wave response excited by active seismic sources in mineral geological exploration. Although exploration signals exhibit random low frequencies after being filtered by geological layers, the wave characteristics such as reflection, refraction, and dispersion contained in them have homology with the transient vibrations induced by mechanical faults in terms of physical mechanisms. Therefore, this type of public dataset can be used to verify the effectiveness of acquisition and processing methods. To evaluate the effectiveness of the proposed method in typical scenarios, a representative mineral was selected as an example for analysis in the experiment. The physical properties of minerals, such as density, hardness, and brittleness, are directly reflected in the mechanical vibration signal characteristics they generate. Their signals are both complex and typical, making them suitable as benchmark cases for verifying EEMD preprocessing and subsequent classification processes. After obtaining the corresponding signal of the mineral, preprocess it using EEMD decomposition. After the decomposition preprocessing, the IMF component was obtained. Since the components with correlation coefficients less than 0.3 are useless components, the correlation coefficients of these components also need to be calculated to eliminate the useless components. The final filtered components are IMF1$\sim$4, which realize the effective noise reduction.

To verify the superiority of the proposed method, it is compared with Backpropagation (BP), CNN and Whale Optimization Algorithm (WOA) in the experiments [23–25]. The cross-entropy loss function was chosen for the experiments. The loss function and accuracy results of the proposed method and the comparison model are shown in Fig. 4. In Fig. 4(a), the loss function values of both the proposed method and the comparison model decreased significantly, indicating that when the number of training sessions increased, the performance of the model improved. The proposed method had the lowest final loss value of 0.075. In Fig. 4(b), the accuracy of both the proposed method and the comparison model increased, indicating that when the number of training times increased, the performance of the model improved. The proposed method had the highest accuracy of 99.2%. This was due to the fact that the neural network contained in the proposed method was able to continuously learn the data features during training, which improved the final result.

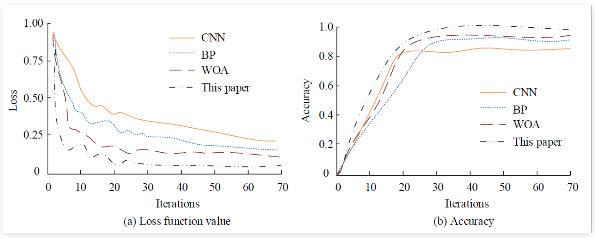

Fig. 4. Loss function and accuracy results

To further validate the accuracy of the proposed methods, Mean Absolute Error (MAE) and Root Mean Squared Error (RMSE) were chosen for the experiments. The results of MAE and RMSE for each method are presented in Fig. 5. The MAE vs. RMSE of each method showed a decreasing trend when the training was increased. However, the proposed method had the lowest MAE vs. RMSE values of 0.38% and 0.094% respectively. The key advantage of this method over BP, CNN, and WOA algorithms lied in its system design for vibration signal characteristics. Compared with BP networks that rely on artificial features and CNN sensitivity to noise, this method obtained physically meaningful IMF components through EEMD adaptive decomposition, providing more important feature inputs for subsequent CNNs. In addition, unlike general optimization algorithms such as Greylag Goose optimization used in references [26] and [27], the EEMD-CNN collaboration mechanism of this method directly starts from the essence of the signal and effectively preserves frequency domain features related to mineral physical properties through decomposition and reconstruction.

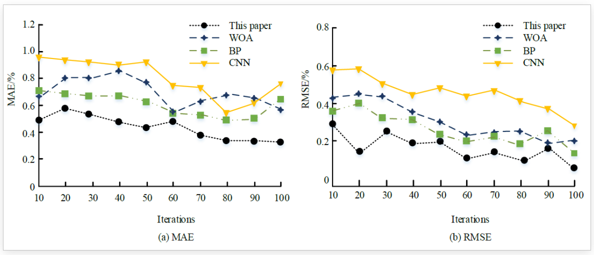

Fig. 5. MAE and RMSE results

To verify the rationality of selecting VGG16 as the classification backbone network, this study compared its performance with ResNet-18 and MobileNet-V2 under the same EEMD preprocessing conditions. The results are shown in Table 1.

Table 1. Architecture comparison under identical EEMD preprocessing

Model	Accuracy (%)	Params (M)	Inference (ms)
VGG16	99.0	138.4	0.070
ResNet-18	97.8	11.7	0.048
MobileNet-V2	96.2	3.5	0.032

According to Table 1, the accuracy of VGG16 (99.0%) was higher than that of ResNet-18 (97.8%) and MobileNet-V2 (96.2%). Although VGG16 had a large number of parameters (138.4M) and a long inference time (0.070ms), it was still within the acceptable range of edge nodes. Considering the strict requirements for classification accuracy in mineral exploration, the accuracy gain of VGG16 was sufficient to compensate for the computational cost, so choosing VGG16 had certain rationality.

4.2. Synchronous triggering and performance comparison of optimized mechanical data acquisition methods

To further verify the performance of the research algorithm in mineral geological exploration data collection, the algorithms in literatures [9], [11] and [13] were selected for comparison. For quantitative comparison, the following evaluation criteria were set: error rate (below 1% is excellent, $1-3\%$ is moderate, and above 3% is poor); Processing speed (less than 150 ms is efficient, 150-200ms is moderate, and greater than 200ms is inefficient); Accuracy (higher than 95% is considered high, 90-95% is considered moderate, and lower than 90% is considered low); Delay (less than 0 ms is considered low delay, $50-100$ ms is considered moderate delay, and greater than 100ms is considered high delay). Each method was independently repeated 10 times, and the results were reported as "mean ± standard deviation". One way analysis of variance (ANOVA) and Tukey post hoc test were used to compare the various indicators between groups, with the proposed algorithm as a reference. Table 2 shows the comparative results of data processing performance indicators of each method.

From Table 2, the designed algorithm had the lowest error rate (0.31%) and the best performance in terms of accuracy. The designed algorithm had the fastest processing speed (120 ms), which was suitable for the application scenarios requiring high real-time performance. The designed algorithm had the highest accuracy (99.5%) and had obvious advantages in reliability. The proposed algorithm had a minimum delay (49 ms) and a fast response time. In addition, compared with the teacher learner optimization algorithm adopted in reference [9], the path aware synchronization mechanism proposed in this study was specifically designed for spatially distributed nodes, effectively solving the time synchronization problem in multi node data collection. Unlike the approach of optimizing noise shaping at the circuit level in reference [11], this study used EEMD-CNN to directly suppress complex noise in the exploration site at the signal level, which had stronger adaptability and flexibility. Compared with the device goal of pursuing high-precision and low-power conversion in reference [13], this study focused on building an end-to-end processing system from synchronous acquisition to intelligent classification, which is more in line with the actual exploration task requirements. Subsequently, the calculation cost of the proposed methods based on ADC, EEMD and CNN was compared and analyzed with other similar methods in the experiment, and the results are shown in Table 3.

According to Table 3, the proposed method (ADC + EEMD + CNN) had a data processing time of 0.400 seconds, which was better than EEMD method and BP neural network, but slightly higher than traditional ADC method and CNN method. This indicated that the combination of EEMD and CNN increased the processing time, but the overall was still within a reasonable range. The proposed method had a CPU utilization of 25.0%, GPU utilization of 40.0% and memory utilization of 150.0MB, which was between the traditional ADC method and the CNN method, showing moderate computing resource requirements. The training time of the model was 8.0min and the reasoning time was 0.070 SEC, which was significantly better than BP neural network, and had obvious advantages in training and reasoning efficiency.

4.3. Experimental Deployment and Verification Results

To verify the practical effect of the mechanical data acquisition method based on ADC and EEMD-CNN in mineral exploration, this study selected the publicly available mechanical vibration datasets on the Kaggle platform (for example: (Mechanical Failure Vibration Dataset), this dataset contains multiple types of mechanical vibration signals and is suitable for simulating the processing scenarios of multi-source heterogeneous data in mineral exploration. The experimental deployment process is as follows:

1. Obtain vibration signal data from Kaggle, standardize it (normalize the amplitude to [-1, 1]), simulate the ADC hardware acquisition process, and generate

Table 2. Comparison results of data processing performance indicators of each method

Index	Literature [9]	Literature [11]	Literature [13]	Designed algorithm
Error rate (%)	1.31 ± 0.12*	2.08 ± 0.18*	3.47 ± 0.25*	0.31 ± 0.04
Processing speed (ms)	139.2 ± 5.1*	178.6 ± 6.3*	198.7 ± 7.2*	119.5 ± 4.6
Accuracy (%)	95.8 ± 0.6*	92.5± 0.8*	89.4 ± 1.1*	99.5 ± 0.3
Delay (ms)	58.7 ± 3.8*	74.9 ± 4.5*	90.1 ± 5.3*	48.6 ± 3.2
Data processing capability	Medium	Medium	Low	High

Note: "*" indicates a significant difference compared with the algorithm used in this study, with $p < 0.05$.

Table 3. Calculation cost results of different methods

Method	Data processing time (s)	CPU Usage (%)	GPU Usage (%)	Memory usage (MB)	Model training time (min)	Model inference time (ms)
Traditional ADC method	0.200	10.0	0.0	50.0	0.1	0.050
EEMD method	0.500	20.0	0.0	100.0	1.0	0.100
CNN method	0.300	30.0	50.0	200.0	10.0	0.080
Proposed method	0.400	25.0	40.0	150.0	8.0	0.070
BP neural network	0.600	28.0	0.0	120.0	15.0	0.120
Whale optimization algorithm	0.550	22.0	0.0	110.0	12.0	0.110

a digital signal sequence of 1024 points per sample with a sampling rate of 10 kHz . 2.EEMD noise suppression: Add Gaussian white noise with an amplitude standard deviation of $\frac{1}{4}$ to each signal segment, perform EEMD decomposition, calculate the correlation coefficients between each IMF component and the original signal, eliminate the components with correlation coefficients lower than 0.3, and reconstruct the effective signal. 3. Feature Classification and Model Training: The VGG16 network is used as the classifier, with denoised signal fragments (converted to time-frequency graph representation) as the input. From the perspective of method applicability, EEMD does not require the adaptive decomposition characteristics of pre-set basis functions and can capture non-stationary random fluctuations in geological signals. CNN automatically learns local feature structures in time-frequency maps through convolutional kernels, without relying on whether the signal has periodicity. The experimental deployment does not rely on simple fitting of specific frequencies or waveforms, so the conclusions obtained can be theoretically extended to low-frequency random vibration scenarios. The time-frequency conversion uses Short Time Fourier Transform (STFT), with a Hamming window length of 256 points and an overlap rate of 75%, to generate a normalized spectrogram of 224 × 224 pixels as input for CNN. Five-fold cross-validation is adopted, the optimizer is Adam, and the loss function is cross-entropy. The model is trained for 100 epochs with a batch size of 32. The initial learning rate is 0.001 and decays by 0.1 times every 20 epochs. The VGG16 fully connected layer consists of a 4096-4096-4 structure, with ReLU as the activation function and Softmax as the output layer activation function. The experimental deployment and verification results are shown in Table 4.

Table 4 verifies the ADC and EEMD-CNN methods based on public vibration datasets. Their average classification accuracy on three different sample sets of various scales reached 99.0%, with MAE and RMSE values of 0.38% and 0.093% respectively, significantly outperforming traditional BP neural networks, single CNNS, and WOA optimization methods. The results confirmed that EEMD could effectively suppress complex vibration signal noise and retain mineral feature information, while the VGG16 network had excellent hierarchical feature extraction performance. After EEMD processing, the average SNR of the signal was increased by 13.1dB, making it suitable for strong noise scenarios in mineral exploration. The average processing latency was 49.3ms, meeting the requirements

Table 4. Experimental Deployment and Verification Results

Experimental Group	Sample size	Accuracy rate (%)	MAE (%)	RMSE (%)	SNR improvement (dB)	Processing delay (ms)
1	1024	98.7	0.41	0.098	12.3	46
2	2048	99.1	0.38	0.092	13.1	49
3	4096	99.3	0.36	0.088	13.8	53
Average	/	99.0	0.38	0.093	13.1	49.3

Table 5. Confusion matrix and F1-score

Class	Predicted A	Predicted B	Predicted C	Predicted D	F1 score
True A	98	1	1	0	0.985
True B	1	97	2	0	0.970
True C	0	2	96	2	0.960
True D	0	0	1	99	0.985
Macro Avg	-	-	-	-	0.989

Note: A, B, C, and D respectively represent four types of mineral vibrations.

of most real-time data acquisition. Although EEMD decomposition and CNN reasoning increase computational overhead, the dual buffering mechanism and synchronous triggering strategy ensured a high response speed of the system. Further analysis of the confusion matrix and F1 scores for each category in the test set is shown in Table 5.

From Table 5, the macro average F1 score was 0.989, and a few misjudgments were concentrated in mineral types with similar vibration characteristics (1-2 cases of confusion between A and B, and 1-2 cases of confusion between C and D). There was no serious confusion between categories. Combined with the 50% verification results in Table 5, significant overfitting could be ruled out.

5. Conclusions

This study proposed a synchronous acquisition architecture based on commercial ADC hardware, path aware time compensation, and double buffering mechanism for mechanical vibration signal acquisition and processing. It constructed an EEMD-CNN collaborative signal processing framework. Through systematic experiments and comparative analysis, the following main conclusions were drawn:

(1) The proposed method achieved a data acquisition accuracy of 0.7% -3.1% amplitude error and 0.05% − 0.30% frequency error at a typical 10 KHz sampling rate, and achieved an accuracy of 99.2%.

(2) The average classification accuracy on sample sets of different scales reached 99.0%, with MAE and RMSE values of 0.38% and 0.093%, respectively. After EEMD decomposition and IMF screening, the average SNR was improved by 13.1 dB.

(3) Compared with the parallel ADC scheme in reference [9] and the noise shaping approach in reference [11], the proposed method solves the problem of multi node asynchronous triggering and complex noise interference through path aware synchronization mechanism and EEMD-CNN signal hierarchy denoising. It has significant advantages in key performance indicators such as error rate (0.31%), classification accuracy (99.5%), and processing delay (49.3ms). Compared with the hardware architecture optimization in reference [13], this study constructed an end-to-end system from synchronous acquisition to intelligent classification, which is more in line with practical exploration needs.

In practical deployment, the system can be applied to scenarios such as slope microseismic monitoring, real-time diagnosis of drilling processes, and early warning of underground goaf collapse. By synchronously collecting vibration signals from multiple nodes and processing them in real-time through EEMD-CNN, it is possible to identify weak vibration patterns related to geological disaster precursors in strong noise backgrounds, providing high-precision decision-making basis for sub millisecond response delay for mining area safety warning. However, the experimental validation of this study mainly relies on publicly available bearing/gear vibration datasets and has not yet taken into account the coupling effects of complex factors such as soil attenuation and environmental seismic noise on the random low-frequency characteristics of signals in real mineral exploration. The performance of this method in strong attenuation and high noise real scenarios still needs to be tested. Meanwhile, the computational overhead caused by EEMD iterative decomposition and VGG16 network also constitutes a constraint on edge deployment. Therefore, in future research, long-term field tests can be further conducted in typical mining areas to establish a true signal benchmark that includes geological attenuation and seismic noise characteristics. Future research can introduce preprocessing of geological absorption attenuation compensation and data augmentation based on environmental noise models to improve the generalization ability of the model. At the same time, future research will explore the EEMD lightweight online solution and adopt efficient network and pruning technologies such as MobileNet to reduce computing and storage requirements, thereby promoting the engineering implementation of this method in unmanned exploration.

References

[1] Q. Qiu, B. Wang, K. Ma, H. Lü, L. Tao, and Z. Xie, (2023) *"A practical approach to constructing a geological knowledge graph: A case study of mineral exploration data"* **Journal of Earth Science** ***34***(5): 1374–1389. DOI: 10.1007/s12583-023-1809-3.

[2] J. Misiak, (2022) *"Geological exploration of the Moon"* **Gospodarka Surowcami Mineralnymi** ***38***(4): 91–104. DOI: 10.24425/gsm.2022.144095.

[3] H. Rajadurai and U. D. Gandhi, (2022) *"A stacked ensemble learning model for intrusion detection in wireless network"* **Neural Computing and Applications** ***34***(18): 15387–15395. DOI: 10.1007/s00521-020-04986-5.

[4] P. P. Groumpos. "A critical historic overview of artificial intelligence: issues, challenges, opportunities, and threats". In: *Artificial Intelligence and Applications*. ***1***. 4. 2023, 181–197. DOI: 10.47852/bonviewAIA3202689.

[5] C. Liu, X. Fu, Y. Li, H. Wang, L. Sun, J. Lu, J. Li, Y. Sun, L. Shi, H. Hu, H. Yuan, and Z. Yang, (2023) *"Petroleum exploration breakthrough and geological significance in Cretaceous Yingcheng and Denglouku formations of Shuangcheng area, northern Songliao Basin, NE China"* **Petroleum Exploration and Development** ***50***(1): 72–84. DOI: 10.1016/S1876-3804(22)60370-7.

[6] B. Chaudhari, (2022) *"Role of swarm intelligence algorithms on secured wireless network sensor environment-A comprehensive review"* **International Journal of Performability Engineering** ***18***(2): 92–100. DOI: 10.23940/ijpe.22.02.p3.92100.

[7] E. Suganya and S. Sountharrajan, (2022) *"Gradient boost-modified classifier with particle swarm optimization and stochastic diffusion search method for data optimization in wireless sensor networks"* **Adhoc & Sensor Wireless Networks** ***54***(3/4): 193–218. DOI: 10.32908/ahswn.v54.9811.

[8] A. A. Elsway, A. M. Khedr, O. Alfawaz, and W. Osamy, (2023) *"Energy-aware disjoint dominating sets-based whale optimization algorithm for data collection in WSNs"* **Journal of Supercomputing** ***79***(4): 4318–4350. DOI: 10.1007/s11227-022-04814-8.

[9] M. V. N. Chakravarthi and B. Chandramohan, (2022) *"Calibration of mismatches in time-interleaved adcs using teacher learner-based optimization algorithm"* **Journal of Circuits, Systems and Computers** ***31***(09): 1–14. DOI: 10.1142/S0218126622501638.

[10] S. Huang, X. Sun, X. Peng, H. Jiang, and S. Yu, (2022) *"Achieving high in situ training accuracy and energy efficiency with analog non-volatile synaptic devices"* **ACM Transactions on Design Automation of Electronic Systems** ***27***(4): 1–19. DOI: 10.1145/3500929.

[11] Y. Zhang, S. Liu, Y. Liang, and Z. Zhu, (2022) *"A 2nd-order noise shaping SAR ADC realizing NTF zero-pole optimization based on IIR-FIR filter"* **Chinese Journal of Electronics** ***31***(1): 33–39. DOI: 10.1049/cje.2020.00.309.

[12] A. Sardar, S. Dey, and S. MISR, (2022) *"An innovative FPGA-based ADC/DAC design using 1-bit adaptive-delta modulation"* **I-Manager's Journal on Circuits & Systems** ***10***(2): 1–9. DOI: 10.26634/jcir.10.2.18902.

[13] S. Bashir, N. U. D. Hakim, and G. M. Rather, (2023) *"Analog-to-digital converters: a review of existing architectures and a new proposal for high resolution sensors"* **Sensor Review** ***43***(2): 125–130. DOI: 10.1108/SR-09-2022-0369.

[14] A. I. Al-Sulaifanie, B. K. Al-Sulaifanie, and S. Biswas, (2022) *"Recent trends in clustering algorithms for wireless sensor networks: A comprehensive review"* **Computer Communications** ***191***: 395–424. DOI: 10.1016/j.comcom.2022.05.006.

[15] Y. Zhang, L. Liu, M. Wang, J. Wu, and H. Huang, (2022) *"An improved routing protocol for raw data collection in multihop wireless sensor networks"* **Computer Communications** ***188***: 66–80. DOI: 10.1016/j.comcom.2022.02.016.

[16] M. Ajoudani, A. Shiekholeslami, and A. Zakariazadeh, (2022) *"Improving state estimation accuracy in active distribution networks by coordinating real-time and pseudo-measurements considering load uncertainty"* **IET Generation, Transmission & Distribution** ***16***(8): 1620–1638. DOI: 10.1049/gtd2.12388.

[17] D. T. Al-Zuhairi, A. S. Hameed, and I. S. Hameed, (2022) *"Dual-stage SVD basis approach for ECG signal associated noise removal"* **Signal, Image and Video Processing** ***16***(6): 1489–1496. DOI: 10.1007/s11760-021-02102-1.

[18] M. Wang, C. Xiong, and Z. Shang, (2025) *"Predictive evaluation of dynamic responses and frequencies of bridge using optimized VMD and genetic algorithm-back propagation approach"* **Journal of Civil Structural Health Monitoring** ***15***(1): 173–190. DOI: 10.1007/s13349-024-00833-6.

[19] B. Heythem, M. Djerioui, T. Beghriche, A. Zerguine, and A. Beghdadi, (2024) *"Customized CNN for multi-class classification of brain tumor based on MRI images"* **Arabian Journal for Science and Engineering** ***49***(12): 16903–16918. DOI: 10.1007/s13369-024-09284-z.

[20] R. Chavez, D. Colosi, H. Salehi, M. A. Ayala, M. L. Chairez, and M. Mahdian, (2025) *"Convolutional neural network—assisted detection of pantomographic technique errors"* **Oral Surgery, Oral Medicine, Oral Pathology and Oral Radiology** ***139***(3): e77–e78. DOI: 10.1016/j.oooo.2024.11.028.

[21] A. Jain, V. Bhatnagar, A. C. S. Rao, and M. Khari, (2023) *"Retina disease prediction using modified convolutional neural network based on Inception-ResNet model with support vector machine classifier"* **Computational Intelligence** ***39***(6): 1088–1111. DOI: 10.1111/coin.12601.

[22] L. Jian, X. Wang, S. Huang, H. Hao, X. Zhang, and X. Yang, (2024) *"Comparative analysis of different empirical mode decomposition-kind algorithms on sea-level inversion by GNSS-MR"* **Journal of Applied Geodesy** ***18***(1): 133–152. DOI: 10.1515/jag-2023-0027.

[23] S. R. Bandi, M. Anbarasan, and D. Sheela, (2022) *"Fusion of SAR and optical images using pixel-based CNN"* **Neural Network World** ***32***(4): 197–213. DOI: 10.14311/NNW.2022.32.012.

[24] G. Luo, (2022) *"Neural network-based optimization model for sprint data collection"* **Journal of Computational Methods in Science and Engineering** ***22***(1): 253–263. DOI: 10.3233/JCM-215729.

[25] A. A. Elsway, A. M. Khedr, O. Alfawaz, and W. Osamy, (2023) *"Energy-aware disjoint dominating sets-based whale optimization algorithm for data collection in WSNs"* **Journal of Supercomputing** ***79***(4): 4318–4350. DOI: 10.1007/s11227-022-04814-8.

[26] E. S. M. Elkenawy, A. A. Alhussan, D. S. Khafaga, Z. Tarek, and A. M. Elshewey, (2024) *"Greylag goose optimization and multilayer perceptron for enhancing lung cancer classification"* **Scientific Reports** ***14***(1): 1–23. DOI: 10.1038/s41598-024-72013-x.

[27] A. E. S. Saqr, M. S. Saraya, and E. S. M. El-Kenawy, (2025) *"Enhancing CO2 emissions prediction for electric vehicles using Greylag Goose Optimization and machine learning"* **Scientific Reports** ***15***(1): 1–38. DOI: 10.1038/s41598-025-99472-0.